ACS APPLIED MATERIALS & INTERFACES

Research Article

www.acsami.org

Spontaneous Water Oxidation at Hematite (α-Fe_2O_3) Crystal Faces

S. Chatman,*[,†,§] P. Zarzycki,[‡] and K. M. Rosso*[,†]

[†]Physical Sciences Division, Pacific Northwest National Laboratory, Richland, Washington, United States

[‡]Institute of Physical Chemistry, Polish Academy of Sciences, Warsaw, Poland

Supporting Information

ABSTRACT: Hematite (α-Fe_2O_3) persists as a promising candidate for photoelectrochemical water splitting, but a slow oxygen evolution reaction (OER) at its surfaces remains a limitation. Here we extend a series of studies that examine pH-dependent surface potentials and electron-transfer properties of effectively perfect low-index crystal faces of hematite in contact with simple electrolyte. Zero-resistance amperometry (ZRA) was performed in a two electrode configuration to quantify spontaneous dark current between hematite crystal face pairs (001)/(012), (001)/(113), and (012)/(113) at pH 3. Exponentially decaying currents initially of up to 200 nA were reported between faces over 4 min experiments. Fourth-order ZRA kinetics indicated rate limitation by the OER for current that flows between (001)/(012) and (001)/(113) face pairs, with the (012) and (113) faces serving as the anodes when paired with (001). The cathodic partner reaction is reductive dissolution of the (001) face, converting surface Fe^{3+} to solubilized aqueous Fe^{2+}, at a rate maintained by the OER at the anode. In contrast, OER rate limitation does not manifest for the (012)/(113) pair. The uniqueness of the (001) face is established in terms of a faster intrinsic ability to accept the protons required for the reductive dissolution reaction. OER rate limitation inversely may thus arise from sluggish kinetics of hematite surfaces to dispense with the protons that accompany the four-electron OER. The results are explained in terms of semiquantitative energy band diagrams. The finding may be useful as a consideration for tailoring the design of polycrystalline hematite photoanodes that present multiple terminations to the interface with electrolyte.

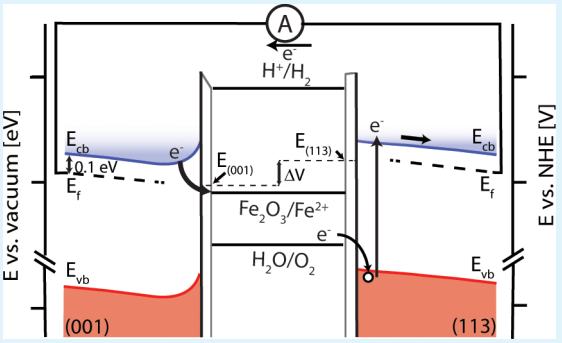

KEYWORDS: *water-splitting, single crystal, photoelectrochemical cell, protonation, oxygen evolution reaction, α-Fe_2O_3*

INTRODUCTION

The unique optical and electronic properties of hematite (α-Fe_2O_3) place this material among the most important of all in the energy-conversion literature.[1−7] For example, hematite has been examined in the role of photoanode for solar water splitting for almost 40 years.[8] Photoelectrochemical cells (PECs) use photogenerated electron−hole pairs to split water into H_2(g) and O_2(g), with the goal of storing energy in H_2(g) for later use in energy production.[9,10] The band gap of hematite ($E_g \approx 2.2$ eV) allows a large portion of the AM1.5 solar spectrum to be used to create photogenerated electron−hole pairs. For n-type hematite, holes migrate to the interface with aqueous solution and are oxidizing enough to accept an electron from water for the oxygen evolution reaction (OER).[1] Because its flat band potential is too low, an overpotential is applied to boost photogenerated electrons to perform the hydrogen evolution reaction (HER) at a suitable cathode elsewhere.[1,11] The H_2(g) and O_2(g) products are kept separate and collected. Device optimization efforts attempt to minimize the overpotential required and maximize the photocurrent yield.

Although hematite exhibits many of the aspects for an ideal photoanode, unfortunately it also suffers practical disadvantages. It has a low optical absorption coefficient, very low hole and electron mobilities, and very high electron−hole pair recombination rates.[1,7,12−15] Strategies to structure hematite into high interfacial area morphologies that maximize light absorption and minimize carrier diffusion lengths have been somewhat successful to overcome these bulk property limitations.[7,15−17] However, the properties of hematite surfaces themselves now appear to be the main performance limitation. In particular, a high concentration of surface states is thought to lead to a larger than expected overpotential until the onset of water oxidation photocurrent; holes become trapped at surface defects.[18] Moreover, OER kinetics at hematite surfaces are unusually slow compared to other metal oxides.[1] As a result, research emphasis is now focused on surface modification, such as by altering the hematite preparation method or by coating the surface with additives to catalyze the OER.[7,15,19,20]

Despite this new emphasis, the underlying electrochemical behavior of ideal hematite surfaces remain insufficiently understood. Constitutive relationships between the atomic structure of a hematite surface in contact with water and its electrochemically observable properties are still not well-

Received: October 1, 2014
Accepted: December 15, 2014
Published: December 15, 2014

DOI: 10.1021/am5067783
ACS Appl. Mater. Interfaces 2015, 7, 1550−1559

known. An observable property relevant to charge-carrier separation and transport is the surface electrochemical potential (ψ_0), which is defined by the thermodynamic equilibrium between the arrangement of surface atoms, the intrinsic tendencies of those atoms to react with water (e.g., protonation/deprotonation), and the pH of the aqueous solution. This characteristic is important for the OER, for example, because at a given hematite termination at a given pH it will set the interfacial electrostatics that govern hole carrier transport across that interface to oxidize water molecules. Recent studies have shown that for three common low-index terminations of hematite, namely, the (001), (012), and (113) faces, differences in ψ_0 on the order of ±100 mV exist at pH extremes of hematite stability.[21−24] Single-crystal hematite surfaces can be expected to be dominantly terminated by hydroxyl groups coordinated with subsurface iron atoms in aqueous environments, although the dependence on surface preparation methods and pH are not well-known.[25−31] Differences in potential arise because different Fe−O bonding topologies are presented to the electrolyte by different terminations of the corundum-type structure. When charge neutral, the (001) face is terminated by hydroxyl groups doubly coordinated to subsurface iron atoms, which are valence saturated and thus have a low proton affinity.[22] The (012) face is terminated in 50% singly coordinated and 50% triply coordinated hydroxyl groups, arranged in a corrugated fashion, with singly and triply coordinated groups exhibiting the highest and intermediate proton affinities, respectively.[21,22,28,30,32] The (113) face has a ratio of 1:1:2 of singly, triply, and doubly coordinated sites, respectively. The pH values of the point of zero potential (PZP) for these faces are in the range from 8.35 to 8.85, but none are equivalent.[21,22]

In principle, these electrochemical differences suggest that for any hematite photoanode morphology bearing multiple terminations, for example, as nanoscale domains in polycrystalline hematite, surface potential gradients exist across domains of the photoanode itself. Conceptually such gradients would be capable of biasing hole accumulation to a specific subset of domains, favoring the OER at only a fraction of the available interfacial area. To which subset and to what extent will depend mainly on the relative proportion of domains and the pH. Given the typical practice of driving PEC water splitting at extremely high pH to avoid higher iron oxide solubility at low pH,[9,33] surface potential gradients across the photoanode could be substantial. In addition to affecting the equilibrium potential, because of steric effects the different bonding topologies at the interface impart distinct kinetics of protonation/deprotonation to hematite faces.[21,22,24,34] Conceptually this distinction could factor into the kinetics of interfacial electron transfer reactions that are coupled to proton transfer or involve proton products that must be transported away from the interface to continue the reaction, such as the OER.[9] These considerations appear germane to the topic of hematite photoanode performance, but to our knowledge they have yet to be studied in a systematic way, such that they could be further explored for photoanode design.

The objective of the present study is to quantify the magnitude and rate of any electrochemical (dark) current that spontaneously flows between individual hematite faces, in contact with a common aqueous electrolyte at a given pH, and to isolate the relevant electrochemical reactions. As was done in a single hematite electrode open-circuit potential study,[21,22,24,35−40] the measurements here were performed on carefully prepared single-crystal single-face hematite electrodes, bearing nearly topographically perfect terminations of known crystallographic orientation and surface area. We report zero resistance amperometry (ZRA) measurements of the current flow between two hematite face electrodes as a function of face pair and time. While motivated by the need to better understand hematite photoanode behavior, for simplicity, we restricted our study to analysis of the spontaneous dark current. The electrolyte composition was chosen to be pure dilute aqueous $NaNO_3$, free of extraneous dissolved gases (e.g., CO_2, O_2) that can interfere with the standard reaction and interfacial potentials,[41] titrated to pH 3 using HNO_3. Low pH was emphasized to simultaneously achieve both a large potential gradient and, given the low partial pressure of O_2, to avoid conditions where magnetite becomes a stable surface reconstruction on hematite.[18,42,43] Although hematite becomes significantly more soluble below pH ≈ 4,[41] the dissolution rate is slow and quantifiable with respect to involvement in the ZRA measurements. From the collected data, we demonstrate and rationalize the spontaneous current flow between hematite faces in terms of preferential faces for the OER. The data furthermore suggest that the kinetics of the OER may be controlled by the rate at which a particular hematite surface can accept and redistribute protons that accompany the four-electron water oxidation reaction.

EXPERIMENTAL METHODS

A large natural specular single crystal of hematite, originating from Cada de Pedramine, Congonhas do Campo, Minais Gerais, Brazil, was selected for this study. The crystal was terminated by visually perfect low-index growth faces bearing no significant inclusions of other phases. Individual faces were excised from the crystal using a low-speed wafering saw (IsoMet, Buehler, USA), yielding 5 × 5 × 0.1 mm slabs, each bearing a natural growth face of interest. Single-crystal X-ray diffraction (Philips, X'Pert XRD, Netherlands) was used to determine face orientation; uniform slabs exposing (001), (012), and (113) as-grown faces were thus collected. This approach has the advantage that all faces are derived from the same initial hematite crystal, grown contemporaneously under identical conditions.

The electron transport properties of the bulk hematite crystal were explored using a variety of techniques. Four-point van der Pauw measurements were used to determine the room-temperature resistivity on the crystal to be 2.01×10^6 Ω·cm. Using the empirical formula for determining carrier concentration from room-temperature resistivity, ($C_{imp} = 10^{-2}(R_{298\ K})^{-1}$, where C_{imp} is carrier concentration),[44,45] a carrier concentration estimate of $\sim 2 \times 10^{14}$ cm^{-3} was obtained. This relatively low carrier concentration suggests that the original monocrystal is of high natural purity. Electron microprobe (EMP) analysis confirmed this result, indicating total crystal impurities to be below 0.09 atom %. Hall effect (Quantum Design, Inc. PPMS, USA) measurements were performed for six field strengths (6, 3, 0, −3, −6 T) at 10 K intervals between 250 and 400 K. Hall effect data confirmed n-type semiconduction typical for hematite, in this case most likely due to minor Ti^{4+} substituted for Fe^{3+}.[46]

Oriented growth face slabs exhibited an initial root mean square (rms) roughness of ∼5 nm as measured by atomic force microscopy (AFM). To remove defects at this scale and adventitious surface contaminants, crystal faces were annealed at 1100 °C in air (Barnstead Thermolyne, Thermo, USA) for at least 12 h, yielding ideal Fe_2O_3 surface stoichiometry as determined by X-ray photoelectron spectroscopy.[21,47] The resulting surfaces exhibited well-organized step-terrace topography with an rms surface roughness of ∼0.1 nm by AFM.[21] These structurally and chemically ideal oriented faces of hematite were constructed into single-face electrodes using acrylic electrode bodies and acrylic bonding agents, yielding a sealed hematite electrode tip of ∼16−20 mm^2 of the exposed crystal face. A pool of mercury was used to make the electrical connection to the back of the hematite slab.[21,22]

DOI: 10.1021/am5067783
ACS Appl. Mater. Interfaces 2015, 7, 1550−1559

Physical setup resistances for remaining electrical connections (i.e., hematite/mercury, mercury/carbon, carbon/copper, copper/brass, brass/steel, etc.) are typically considered to be approximately an ohm, such that for the order of magnitude of currents measured in this study (~nanoamperes) the contact resistant potential drops are negligible (~nanovolts) influences on measured potentials (~100 mV). Between electrochemical measurements, crystals were removed and reannealed to reset the face for reuse, as per previous work.[35]

Electrochemical data were recorded with a potentiostat (CH Instruments, Model 660D, USA) in conjunction with a continuously stirred two-electrode cell. Because the objective of the present study was to evaluate nonphotoexcited currents, all experiments were performed in a dark electrochemical cell; the possible complication of light-driven excitation of charge carriers was eliminated. ZRA was used to collect electrical current between three sets of dissimilar hematite face pairs ((001)/(012), (001)/(113), and (012)/(113)). Face-pair measurements were collected by connecting separate single-face electrodes, each of known crystallographic orientation (constructed as per a previously published technique[21,22]), together with leads of known input polarity to the potentiostat in ZRA mode (Supporting Information, Figure S1). All experiments were performed in a nitrogen atmosphere with an oxygen partial pressure below 0.1 ppm. All electrolytes were prepared using ACS-grade reagents (Fisher Scientific, USA) and ultrapure water (>18.2 MΩ·cm, Barnstead Nanopure, USA) degassed by boiling under vacuum for more than 1 h. Electrodes were allowed to equilibrate in separate baths of 100 mM $NaNO_3$ at pH 7 for 12−18 h beforehand to ensure that the surface was completely hydrated.[21] The electrodes were then assembled into a two-electrode cell containing 100 mL of 100 mM $NaNO_3$ and titrated to pH 3 with aliquots of 0.1 HNO_3. Open-circuit potentials between the two faces were collected immediately before the ZRA data to ensure the crystals had come to equilibrium and to record initial potential differences between faces. Control measurements showed that no current flowed between equivalent face pairs to a detection limit of 10 pA. The ZRA data set for each hematite face is the average of at least eight ZRA experiments on that face type, with annealing resets of the surface in-between experiments.

All experiments were performed at room temperature to utilize previously reported data on phase stability,[41] dissolution rates,[48] surface potentials,[21,22] and relative protonation/deprotonation rates.[21]

RESULTS AND DISCUSSION

Thermodynamic Equilibria at Open Circuit. Our aqueous solution conditions were selected to minimize possible redox chemistry and surface reconstructions at the hematite/electrolyte interface. Figure 1 shows the calculated Pourbaix diagram relevant to the open circuit condition in the system at equilibrium and measured surface potentials for hematite (001), (012), and (113) faces at pH 3.[21,22] At these conditions the hematite electrodes lie within the hematite stability field only in the presence of millimolar or greater concentrations of aqueous Fe(II), as defined by the following half-reaction:

$$2Fe^{2+}_{(aq)} + 3H_2O \leftrightarrow Fe_2O_3 + 6H^+ + 2e^-$$
$$E_0[V] = 0.728 - 0.1773pH - 0.0591 \log(Fe^{2+}_{(aq)}) \quad (1)$$

Because no aqueous Fe(II) is included in the solution, the system tendency for dissolution of hematite (i.e., reaction to the left in eq 1) is clear. Equation 1 represents a dissolution reaction that, conceptually, could produce current between inequivalent faces through preferential attack of one face over the other and therefore must be considered relevant to ZRA measurements. Second, because of the potential of the valence band maximum in hematite (ca. −2.5 V vs normal hydrogen electrode (NHE) at pH 3),[49] the OER must also be considered as a possible source of current, by the half-reaction

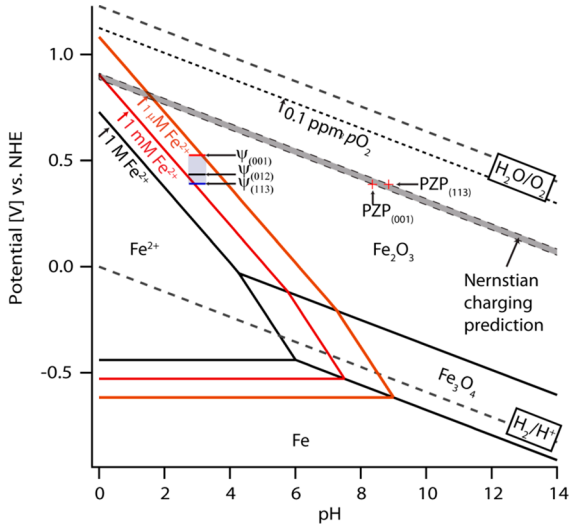

Figure 1. Calculated Pourbaix diagram for the experimental system at equilibrium open-circuit conditions. Measured face-specific hematite surface potentials at pH 3 are shown.[21,22] The Nernstian charging prediction area is based on the slope of −59.1 mV/pH and the PZP values collected for faces studied here.[22]

$$2H_2O \leftrightarrow O_2 + 4H^+ + 4e^-$$
$$E_0[V] = 1.228 - 0.0591pH - 0.0147rO \quad (2)$$

This equilibrium defines the upper stability limit for water; the low partial pressure of O_2 in our system decreases the size of the water stability field, moving the boundary closer to the potentials of the hematite electrodes (Figure 1). Holes near the valence band maximum for hematite are expected to have redox potential of ~2.5 V versus NHE, sufficiently oxidizing to accept electrons in eq 2 and drive this reaction to the right.[1,5] Two final equilibria are conceptually relevant. The hydrogen evolution reaction (HER), as given by

$$H_2 \leftrightarrow 2H^+ + 2e^-$$
$$E_0[V] = 0.000 - 0.0591pH - 0.0295rH \quad (3)$$

can be ruled out in the absence of powerful reductant; as is well-known, electrons at the conduction band minimum of hematite (−0.5 V vs NHE at pH 3) are not sufficiently reducing to drive eq 3 to the left. This deficiency is the reason an overpotential of at least 0.5 V is required to boost conduction band electrons to potentials capable of the HER using hematite as the photoanode in a solar PEC device.[1,9−11] Finally, redox reactions of NO_3^- were considered; 100 mM $NaNO_3$ was used as the background electrolyte. From the standard redox potentials for possible nitrate redox reactions that could be occurring in our system, we found that none were significant at pH 3.[41] The set of equilibria relevant to ZRA measurements thus consists of just eqs 1 and 2, hematite dissolution, and the OER, respectively.

The measured open-circuit potentials of the three hematite faces show a range of ~120 mV at pH 3, with the (001) face the most electropositive, and the (113) face the most electronegative. This range and ordering is similar to that reported by Yanina and Rosso[23] between (001) and (*hk*0) faces at pH 3 in inert electrolyte (KCl). The measured potentials and analysis of the relevant thermodynamic equilibria above suggest that in the ZRA experiments current will flow to the (001) face when

DOI: 10.1021/am5067783
ACS Appl. Mater. Interfaces 2015, 7, 1550−1559

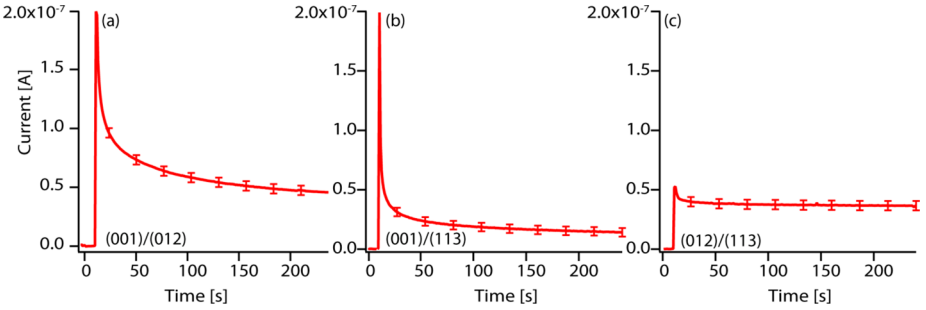

Figure 2. ZRA current data collected for three hematite face pairs. (a) (001)/(012). (b) (001)/(113). (c) (012)/(113). Each curve represents a minimum of eight averaged experiments with identically prepared faces, reannealed between each experiment. Error bars represent 2σ standard deviation.

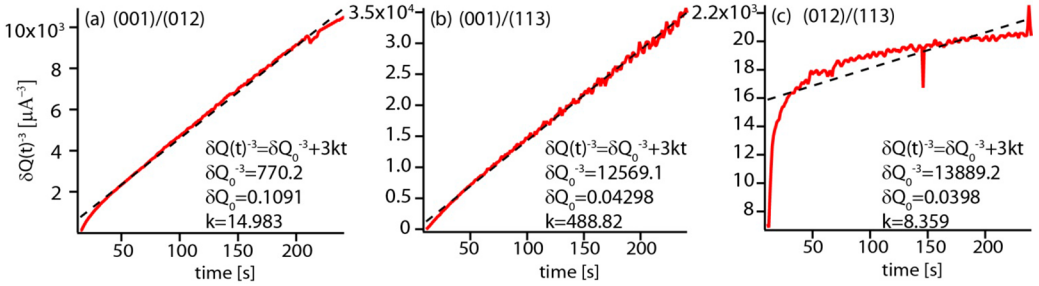

Figure 3. Kinetic analysis of the ZRA data, fitted to eq 5 with $n = 3$ (fourth order) for the (a) (001)/(012), (b) (001)/(113), and (c) (012)/(113) face pairs.

connected to either (012) or (113) and that the current magnitude and kinetics will depend on the interfacial electrochemistry of eqs 1 and 2 only. That is to say that the more electropositive face (001) will be dominated by the reductive dissolution reaction (eq 1) when connected to the more electronegative faces (012)/(113), which will be dominated by the OER (eq 2), based on the system thermodynamics. A schematic diagram of the expected electrochemistry and current flow direction is given in Figure S1. These expectations are directly testable through ZRA measurements, as described below.

Zero Resistance Amperometry. Spontaneous currents in the dark between face pairs at pH 3 are shown in Figure 2. Currents of up to 200 nA (1.25 μA/cm^2) were measured between (001)/(012) and (001)/(113) (Figure 2a,b); the third face pair, (012)/(113), exhibited current of up to 50 nA (0.31 μA/cm^2) (Figure 2c). In all cases, as expected, the current is largest upon closing the circuit, and rapidly decays away with time, in this case over the measured interval of 240 s. A maximum time of 240s was chosen to reduce surface dissolution and avoid long time equilibration reactions.[50−52] For all ZRA measurements the working electrode lead of the potentiostat was connected to the more electropositive of the two crystal faces, as determined by open-cell potential measurements collected immediately prior to current collection (Figure 1). The average pre-ZRA potential differences between faces ($\Delta\psi_{(001)/(012)} = 75 \pm 5$ mV, $\Delta\psi_{(001)/(113)} = 100 \pm 5$ mV, $\Delta\psi_{(012)/(113)} = 35 \pm 5$ mV) measured here were commensurate with those from earlier work ($\Delta\psi_{(001)\text{-}(012)} = 82 \pm 8$ mV, $\Delta\psi_{(001)\text{-}(113)} = 118 \pm 8$ mV, $\Delta\psi_{(012)\text{-}(113)} = 36 \pm 8$ mV).[22] The polarity of the current data in Figure 2 signifies that electrons were injected into the more electronegative face (anode) from solution and flowed to the more electropositive face (cathode) through the potentiostat (see Figure S1). For each set of current data collected a complete circuit is required, thereby requiring both a reduction and an oxidation reaction to be occurring in series at separated faces (electrodes). All three sets of data suggest a slow decay to zero current at time $t \gg 240$s. We believe this is due to a general restructuring of the surface caused by slow hematite dissolution (eq 2) at both surfaces.[50,51] If a complete restructuring were to occur, and each face were transformed to a nonpreferentially oriented polycrystalline state, then the face−face bias (and current) would go to zero. We avoid this by limiting the time to 240 s and refreshing the electrodes with an annealing process between experiments. Below we discuss how the collected ZRA data can be interpreted in terms of the complementary anode and cathode half-reactions, that is, eqs 1 and 2, which complete the circuit. We also construct energy-band diagrams to explain electron transfer through these systems.

The current decay represents the relaxation process of removing an electrostatic potential bias between connected single-crystal electrodes. By analyzing the kinetics we can determine the rate-limiting step in the completed circuit. ZRA data were transformed into time-dependent charge ($Q(t)$) by integrating the current using the following equation:

$$Q(t_0 \rightarrow \tau) = \int_{t_0}^{\tau} [I(t) - I_{res}]\mathrm{d}t \tag{4}$$

where $I(t)$ is the collected current data, t_o is the initial collection start time, τ is the maximum time, and I_{res} is the current at τ. $Q(t)$ can then be inserted into the integrated rate law:

$$-\frac{\mathrm{d}}{\mathrm{d}t}\delta Q(t) = k[\delta Q(t)]^n \tag{5}$$

where k is a real number fitting parameter and n is an integer fitting parameter that gives the order of the rate limiting reaction. By comparing the data to different integer values of n,

DOI: 10.1021/am5067783
ACS Appl. Mater. Interfaces 2015, 7, 1550−1559

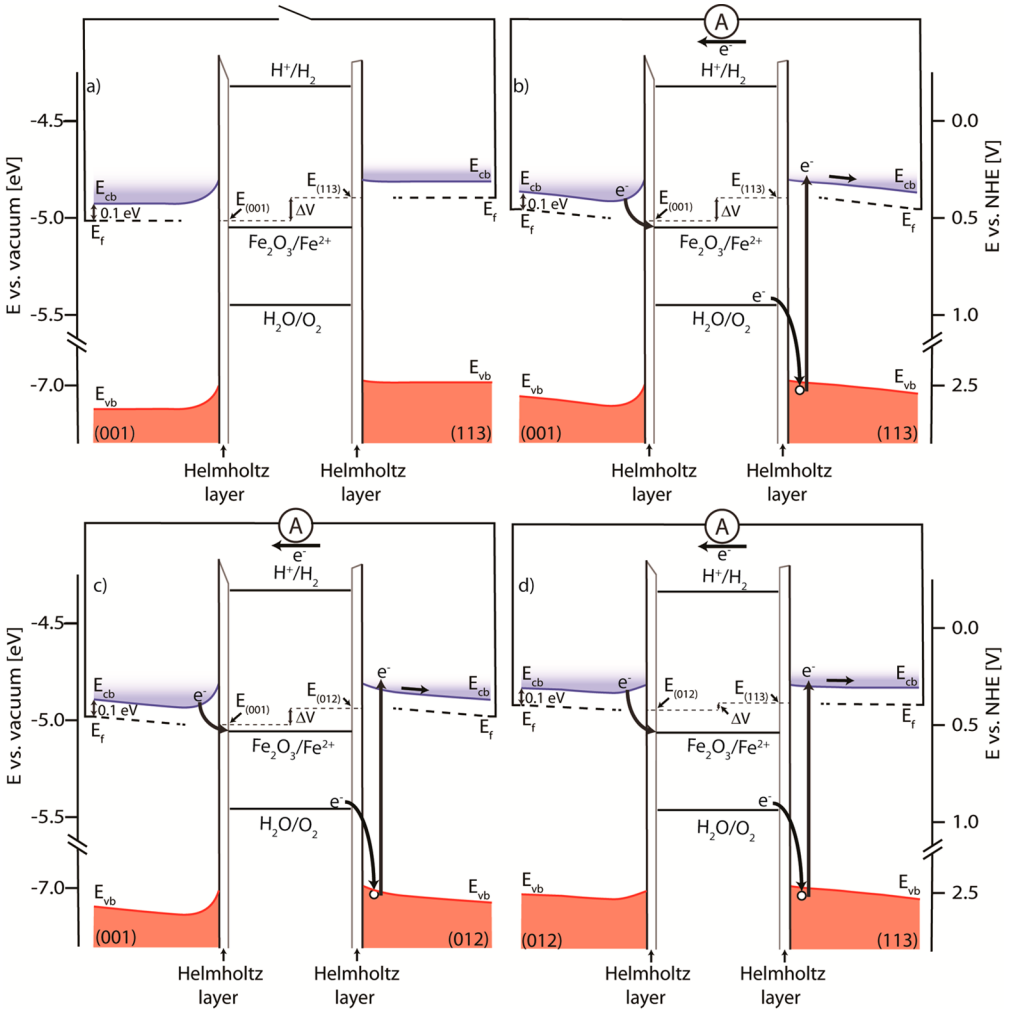

Figure 4. Energy-band diagram before (a) and during (b, c, d) ZRA experiments for three face pairs.

the rate-limiting process can be determined. In particular n can be related to the elementary number of electrons passed during the rate-limiting reaction. Attempts to fit the data to n = 0, 1, 2, and 3, corresponding to first- through fourth-order reactions, respectively, showed poor fits for first-, second-, and third-order kinetics (Supporting Information, Figure S2). As seen in Figure 3a,b, excellent fits are obtained for the two face pairs involving (001) using n = 3, indicating that the rate-limiting reaction for (001)/(012) and (001)/(113) (Figure 3a,b) is of fourth-order character.[53,54] The ZRA data for the (012)/(113) face pair could not be fit to any integer value of n = 0−30, and is certainly not fourth order as in the other two cases (Figure 3c). The fact that the ZRA data for the (012)/(113) face pair does not conform to any integer value of n suggests that neither the reactions listed above (eqs 1−3) nor any other reaction is controlling the reaction rate. There are multiple factors than can result in the failure of kinetic analysis to determine the rate-determining step in a multistep integrated reaction chain.[53,54] The concept of a rate-determining step is only valid if one of the reactions in a series is much slower than the others.[53,54] If two reactions have similar reaction rates there is no clear rate-determining reaction to manifest in rate control in the data. Another possible factor that can exclude integer orders in the kinetic analysis is the effect of slow reactant/product uptake/release at the electrode surfaces. If the diffusion rates to or from the surface are lower than the reaction rate then the reaction is diffusion-controlled and will not manifest bona fide integer orders.[53,54] Below we show surface potential relaxation data suggesting that the proton uptake/release rates of the (012) and (113) faces are statistically equal, and from this we may infer that the lack of fourth-order kinetics for (012)/(113) face pair is because the OER and dissolution reactions have similar kinetics in this case. Furthermore, these similar kinetics may arise from the fact that the proton uptake kinetics (for the dissolution reaction) and the proton release kinetics (for the OER) on these two faces are similar, as discussed below.

This analysis suggests that the flow of current between (001)/(012) and (001)/(113) is controlled by a four-electron transfer reaction stoichiometry, which in this system must correspond to the OER (eq 2). The current polarity indicates that OER electrons flow from the less positive face ((012) or (113)) to the more positive face (001) through the potentiostat. Note that by integrating the current in Figure 2 we can determine the total number of electrons transferred between the face pairs, which for the cases of (001)/(113) and (001)/(012) can be used to determine the amount of molecular oxygen produced at the anode over 4 min. The total number of electrons transferred was $n_{(001)/(012)} = 8.80 \times 10^{13}$ electrons and $n_{(001)/(113)} = 3.03 \times 10^{13}$ electrons ($n_{(012)/(113)} = 5.43 \times 10^{13}$ electrons). This indicates that the OER supplies on the order of 0.25 nmol O_2 (~0.4 molecules of O_2 per nm^2 for comparison) of dissolved molecular oxygen to

DOI: 10.1021/am5067783
ACS Appl. Mater. Interfaces 2015, 7, 1550−1559

the solution over 4 min for the cases of (001)/(113) and (001)/(012). This amount is too low to detect and is expected to disperse into the electrolyte and into the mass of nitrogen atmosphere headspace in the cell without affecting electron-transfer processes at the cathode.

The corresponding cathodic half-reaction must be the hematite dissolution reaction, eq 2, occurring most favorably at the (001) face and without limiting the rate of current flow. While the dissolution rate of hematite (001) at pH 3 in low-oxygen aqueous solution is not specifically known, the bulk hematite dissolution rate in acidic reducing conditions is between approximately 0.1 fmol Fe^{3+}/min (proton-promoted dissolution) and 10 fmol Fe^{2+}/min (reductive dissolution).[48] Taking the reductive dissolution rate and assuming a unit charge for each iron atom released (e.g., $Fe^{3+} \rightarrow Fe^{2+}$), this rate indicates a current of 0.10 pA (for the maximum of 10 fmol/min), 5 orders of magnitude lower than the current recorded in any of the ZRA experiments reported here. Hence the bulk hematite dissolution rate alone initially appears insignificant to account for the observed ZRA current.

Energy-Band Diagrams. The observed behavior can be illustrated in terms of energy-band diagrams for the face pairs, treating each semiconductor−electrolyte interface as the basis for a Schottky junction, before and after the circuit is closed to allow current to flow. The conduction band minimum (E_{cb}) can be set using the value calculated by Xu and Schoonen using electronegativities[49] (−4.78 eV vs vacuum); the electron affinities (i.e., E_{cb} relative to vacuum) are assumed constant.[55,56] We also use the position of the semiconductor Fermi energy relative to the conduction band minimum quoted by Xu and Schoonen. They use 100 meV below E_c (−4.88 eV vs vacuum), in agreement with many calculations of energy band levels of n-type semiconductors and the value used previously in hematite electrode calculations.[16,57−60] This level is also commensurate with the 200 meV activation energy calculated by Rosso et al.[46] for the excitation energy of valence electrons on Fe^{2+} donor sites (originating from Ti^{4+} substitutional dopants). From the band gap of hematite (2.2 eV) we can then calculate the valence band maximum (E_{vb}, −6.78 eV vs vacuum). Together these three values give us the pertinent band levels of bulk hematite in vacuum.

To adjust band positions for contact with pH 3 electrolyte, the Fermi energy at the interface must be known. It is typically assumed that the Fermi energy of the semiconductor would equilibrate to the electrochemical potential (∼Fermi energy) of the electrolyte, which is the average redox potential of eqs 2 and 3 for aqueous solution. This is valid if the system satisfies two criteria: (1) the ionic species in the electrolyte are potential determining ions (PDIs) for the semiconductors, as they are for water species on metal oxide surfaces and (2) the system exhibits Nernstian charging (−59 mV/pH).[57] While H^+ and OH^- are PDIs, the single-face electrodes deviate from Nernstian charging behavior.[21,22,24,35] Therefore, we cannot assume that the Fermi energies of the hematite electrodes coincide with the average redox potential of water stability limits; such an assumption would furthermore be inconsistent with the measured potential difference between faces before the circuit is closed. Instead, we use the surface potentials of the three faces measured via potentiometric titration[21,22] to position the Fermi energy at the surface. At pH 3 $E_{(001)}$ = −5.015 eV, $E_{(012)}$ = −4.933 eV, and $E_{(113)}$ = −4.897 eV versus vacuum ($E_{(001)}$ = 0.515 V, $E_{(012)}$ = 0.433 V, and $E_{(113)}$ = 0.397 V vs NHE[22]).

Band diagrams are shown in Figure 4. Figure 4a indicates the energy levels of the (001) and (113) faces in equilibrium with the electrolyte at pH 3 before the circuit is closed. The band bending at the surface is due to Schottky junction formation as the Fermi energies independently equilibrate across respective electrode/electrolyte interfaces. The initial potential difference (∼120 mV) is displayed as that between face-specific equilibrium Fermi energy levels. Both face terminations will tend toward negative (downward) semiconductor band bending, establishing the built-in electric field that sweeps free excited electrons into the bulk of the semiconductor.[55,56] Redox potentials for eqs 1, 2, and 3 calculated for the bulk electrolyte at pH 3 are also shown.

For the closed-circuit condition, at time zero, reactions that contribute to current flow as the system equilibrates for the three face pairs are shown in Figure 4b−d. The band diagrams are calculated semiquantitatively for each of the three face pairs, (001)/(113) (Figure 4b), (001)/(012) (Figure 4c), and (012)/(113) (Figure 4d). Equilibration of Fermi levels can be expressed as inclined bands throughout the bulk of both hematite electrodes, which drive electrons from the anode to the cathode through the potentiostat. While here we show that the time dependence of the current is limited by the kinetics of the OER, because the measurements were performed in the dark the concentration of conduction-band electrons and valence-band holes is limited to that from thermal promotion across the band gap alone. Thus, the maximum (integrated) current is limited by thermally available carrier densities at the surfaces of each respective electrode. Under illumination, such as in a water-splitting PEC cell, conceptually, the conduction-band electron density and valence-band hole density would be increased through photoexcitation;[9,11] thus, one could expect higher integrated current flow. However, the additional effect of photoexcited electrons could modify the energy-band relationships by shifting the Fermi energies due to a change in the relative electron densities in the valence and conduction bands.[9,55,56] Additional work on the light-driven formation of electrolytic water-splitting products at well-organized single-crystal hematite faces like those here would be needed to unravel such effects.

In addition to the effect of photoexcitation on electron transfer in these systems, the temperature dependence of the ZRA data could also be explored, thereby testing the dependence of the dark current on thermally excited conduction band electrons. We used room temperature here to take advantage of the previous work completed on the surface charging,[21,22,24,34,35] surface protonation/deprotonation rates,[21] and dissolution rates of hematite.[48]

A third technique that could be considered to elucidate more information from this system is the addition of a one-electron hole scavenger, such as hydrogen peroxide.[3] The addition of a hole scavenger during an oxidation reaction is a powerful technique when attempting to explore inefficiencies in photoelectrochemical cells due to charge recombination.[3] In our system, the addition of a hole scavenger would introduce an anodic reaction in parallel with the OER and competitive with it for conduction band holes. If the scavenger was chosen with a hole-scavenging rate faster than the OER, then this technique would chiefly reduce the hole concentration at the anode surface, and the current density from the OER would be subsumed into the hole-scavenger kinetics. However, adding a hole scavenger here would come with added complexities. The hole scavenger would have to be carefully chosen so that it did

DOI: 10.1021/am5067783
ACS Appl. Mater. Interfaces 2015, 7, 1550−1559

not couple with surface adsorbed protons, thereby affecting the surface charge and the inherent system bias. The chosen hole scavenger would also have to exhibit pH-independent activity, thereby eliminating the effect of coupling to hematite dissolution or OER reactants/products on electron transfer through the system. Adding a hole scavenger may help to explicate extra information from this system, but such a set of experiments would require a large set of complementary analyses to understand the system as well as the simpler system studied here.

Electrons in the conduction band near the surface are at an energy level of approximately −4.8 V versus vacuum (0.300 V vs NHE) and so are ∼250 meV more reducing than the standard potential of hematite reduction. We deduce that the cathodic reaction is the hematite reductive dissolution reaction (E_o = 0.550 V vs NHE at pH 3 and an estimated maximum ∼1 μM aqueous Fe^{2+}), eq 1. While there is an energy barrier to overcome (the built-in potential), electrons near the surface can become localized at an Fe^{3+} site to create a surface Fe^{2+}. At pH 3 these hematite faces are well below their PZP values,[21,22] and therefore the inner Helmholtz plane has a net positive charge due to accumulation of protons. This condition creates a tendency for any charge-carrying electrons that impinge on the interface to become trapped at outermost surface iron cations.[61,62] Such ferrous surface atoms will be prone to detach from the surface, akin to eq 1, in combination with surface hydroxyl groups, dissolving the surface.[23] This process is similar to that observed by Yanina and Rosso[23] at the cathode side of hematite monocrystals. The total number of iron atoms can also be determined with the total number of electrons passed during the ZRA experiments. Over the course of the ZRA experiments, current data indicate that on the order of 0.1 nmol of Fe^{2+} is released into the solution (1.6 Fe^{2+} ions per nm^2), a concentration too low to be measured.

Although this rate of Fe^{2+} release at the cathode is much higher than expected from the bulk hematite dissolution rate, as discussed above, the conditions in the present experiments are different. In this case hematite dissolution is occurring under the influence of a cathodic bias, created by connection to the partner surface. The excess electrons biased to the cathodic surface work against the depletion layer and reduce the depletion width. Consequently the Schottky barrier between conduction-band electrons and the redox potential of hematite dissolution will be reduced, accelerating the reductive dissolution rate and allowing eq 1, galvanically driven, to complete the circuit. Although a depletion layer is still expected to persist at the cathode, holes are less available to accumulate at this interface, for converse electrostatic reasons. Holes will be consumed by a higher recombination rate given the excess electron pile-up. Electron pile-up at the cathodic surface will also have a tendency to increase the apparent band gap through the Moss−Burstein effect.[63,64] The reverse current, due to the OER, although thermodynamically feasible, is thus expected to be suppressed at this surface, relative to that at the anode, where the OER (eq 2) dominates the interfacial redox chemistry.

Although all three face pairs show similar cathodic and anodic processes, the kinetics are clearly different for the (112)/(113) face pair, as mentioned. The lack of a reasonable fit with any integer value of n for eq 5 suggests that there is no clear rate-limiting electron-transfer step for this face pair. As mentioned, a possible cause for the more complex kinetics for this face pair relates to protonation/deprotonation kinetics of the various hematite faces. At the anode, the OER involves proton production and release from that interface. Opposite to the OER, the hematite dissolution reaction involves consumption of protons by the surface (eq 1), which liberates Fe^{2+}. We analyzed potentiometric titration hysteresis data previously published for the three hematite faces.[21] By plotting the surface potential versus equilibration time at each pH we were able to determine the relaxation rate (see Supporting Information, Figure S3), which can be interpreted as an indicator of the protonation/deprotonation rate of that face. As seen in Figure 5, the (001) face has a uniquely facile rate of protonation; all

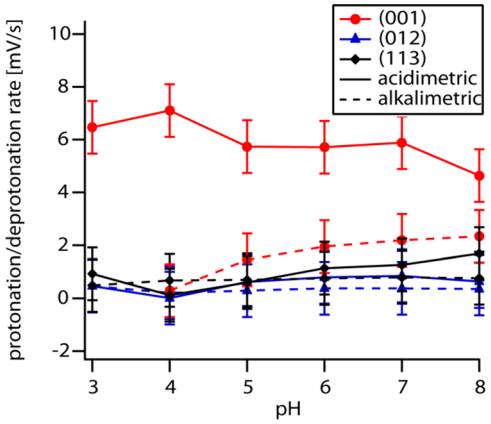

Figure 5. Surface protonation (solid lines) and deprotonation (dashed lines) relaxation kinetics as determined by potentiometric titration hysteresis for the (001) (red ●), (012) (blue ▲), and (113) (black ♦) faces[1].

other rates of protonation/deprotonation are statistically equivalent and slower than (001) protonation at pH 3 by a factor of ∼8. If it is assumed that a principal rate control on the OER and the hematite dissolution reaction is the ability of a surface to facilitate proton transport to/from the interface, a reasonable assumption given that protons are the main charged species that must interact with these net positively charged hematite faces, then the titration rate data suggest uniquely fast hematite reductive dissolution kinetics at the (001) face. This is consistent with the kinetics analysis of the ZRA data, which indicate OER rate limitation for the two face pairs involving (001), with that face taking the role of cathode where eq 1 dominates.

In contrast, the (012) face does not exhibit the facile proton uptake of the (001) face. The failure of the (012)/(113) ZRA data to conform to integer-order kinetics analysis suggests not only that the OER and dissolution reaction rates are similar but also that, when combined with the conclusions from Figure 5, we can infer that the basis for these similar kinetics is the similar protonation and deprotonation rates at these two faces for this cell. From the ZRA data collected from the (001)/(hkl) face pairs we know that the OER is rate-limiting and that this reaction involves proton release from the anodic surface and that both the (012) and (113) faces have similar protonation/deprotonation rates. An interpretation that is comprehensively consistent across all our data is that protonation/deprotonation rates could be the rate-controlling process for both the OER and dissolution reaction for (012) and (113) faces, though it should be noted that the hematite dissolution reaction (eq 1) requires 3 protons per electron transfer (uptake), whereas the OER (eq 2) creates only one proton per electron transfer

DOI: 10.1021/am5067783
ACS Appl. Mater. Interfaces 2015, 7, 1550−1559

(release). As mentioned above, the concept of a kinetic rate-determining step is only valid if there is one reaction in an integrated reaction chain that is significantly slower than the other steps.[53,54] Similar oxidation/reduction rates at the two separated electrodes would lead to convoluted kinetic data, disallowing the use of kinetic analysis in this case.[53,54] Consequently, our data suggest that it is important to study both electron-transfer kinetics and reactant/product uptake rates to fully understand the kinetics of electron transfer at semiconductor electrodes during fuel producing reactions. Our results indicate that exploring proton uptake and release rates as primary controls on electron-transfer kinetics may be an important new consideration.

The OER has previously been linked with the low efficiency of PEC cells involving hematite as the photoanode.[1,2,5,7,15,65] Slow OER kinetics has been attributed predominantly to the low hole mobility and high electron−hole recombination rates observed in hematite, and more recently to hole trapping at surface defects.[1,2,4,5,66] Equation 2 indicates that the OER will produce protons at the surface of the anode. Protons generated at the surface will increase the surface concentration of protons (lowering the effective surface pH) and will thereby shift the redox potential of the OER at the surface (eq 2) more positive (vs NHE), possibly reducing the potential difference between the valence-band maximum of the anode and the redox potential of the OER. From potentiometric titrations[21] we know that the excess protons at the surface will diffuse away at rates comparable to the time scale of the ZRA measurements, suggesting that the deprotonation rate at the surface is a contributing factor to OER reaction kinetics at hematite faces. Such a finding is likely also relevant to the OER under photoanode conditions for hematite.

CONCLUSIONS

We report spontaneous OER current in the dark between pairs of single-face hematite electrodes in inert electrolyte at pH 3. We found that interfacial redox reactions are facilitated by surface potential biases originating from differences in pH-dependent surface charging between faces bearing different atomic topologies to the electrolyte. Kinetics analysis of the current response identified the rate-limiting reaction at the anode as the OER between face pairs involving (001), which was itself found to serve as cathode via relatively faster reductive dissolution. Energy-band diagrams were constructed to explain the face pair cells, from measured surface potentials[21,22] and known energy levels[49] for hematite. By analyzing titration relaxation kinetics for the three hematite faces, we found that the protonation rate of the (001) face is considerably higher than the protonation/deprotonation rates of the (012) and (113) face terminations, suggesting a higher intrinsic ability to accept and redistribute protons on this surface, consistent with the deduced cathodic tendency of the (001) face with respect to (012) and (113). The importance of protonation/deprotonation kinetics for controlling the rate of fuel-producing reactions is reinforced by the observation of more complex amperometry between (012)/(113) faces, where such kinetics is observed to be similar. Our work is the first to explore the separate components of fuel-producing water-splitting reactions at true single-crystal surface terminations. The findings indicate that exploring proton-transfer rates through materials and crystallographic morphology engineering may offer a new avenue of research for increasing fuel-producing reaction rates at device electrodes. With respect to use of hematite at the photoanode in PECs, the collective data suggest that nanoscale domains in polycrystalline hematite will spontaneously partition some of the total useable hole density to a subset of the most anodic domains for the OER. Controlling the type and proportion of such domains could lead to improved photoanode performance.

ASSOCIATED CONTENT

Supporting Information

Electron transfer schematic, fitting of current data to zero-, first-, and second-order charge-transfer kinetics, schematic representation of determining protonation/deprotonation relaxation rates. This material is available free of charge via the Internet at http://pubs.acs.org.

AUTHOR INFORMATION

Corresponding Authors

*E-mail: Kevin.Rosso@pnnl.gov. (K.M.R.)
*E-mail: chatmans@caltech.edu. (S.C.)

Present Address

[§]Joint Center for Artificial Photosynthesis, California Institute of Technology, Pasadena, CA 91125.

Author Contributions

The manuscript was written through contributions of all authors. All authors have given approval to the final version of the manuscript. All authors contributed equally.

Notes

The authors declare no competing financial interest.

ACKNOWLEDGMENTS

This research was supported by the Geosciences Research Program in the U.S. Department of Energy (DOE), Office of Science, Office of Basic Energy Sciences, Division of Chemical Sciences, Geosciences, and Biosciences. It was performed using EMSL, a national scientific user facility sponsored by the DOE Office of Biological and Environmental Research and located at Pacific Northwest National Laboratory, which is a multiprogram national laboratory operated for DOE by Battelle. P.Z. was also supported by Ministerstwo Nauki i Szkolnictwa Wyższego (MNiSW) Grant No. IP2012 059872.

REFERENCES

(1) Sivula, K.; Le Formal, F.; Grätzel, M. Solar Water Splitting: Progress Using Hematite (α-Fe_2O_3) Photoelectrodes. *ChemSusChem* **2011**, *4*, 432−449.

(2) Braun, A.; Sivula, K.; Bora, D. K.; Zhu, J.; Zhang, L.; Grätzel, M.; Guo, J.; Constable, E. C. Direct Observation of Two Electron Holes in a Hematite Photoanode during Photoelectrochemical Water Splitting. *J. Phys. Chem. C* **2012**, *116*, 16870−16875.

(3) Dotan, H.; Sivula, K.; Grätzel, M.; Rothschild, A.; Warren, S. C. Probing the Photoelectrochemical Properties of Hematite (α-Fe_2O_3) Electrodes Using Hydrogen Peroxide as a Hole Scavenger. *Energy Environ. Sci.* **2011**, *4*, 958−964.

(4) Hisatomi, T.; Brillet, J.; Cornuz, M.; Le Formal, F.; Tétreault, N.; Sivula, K.; Grätzel, M. A Ga_2O_3 Underlayer as an Isomorphic Template for Ultrathin Hematite Films Toward Efficient Photoelectrochemical Water Splitting. *Faraday Discuss.* **2012**, *155*, 223−232.

(5) Sivula, K. Metal Oxide Photoelectrodes for Solar Fuel Production, Surface Traps, and Catalysis. *J. Phys. Chem. Lett.* **2013**, 1624−1633.

(6) McKone, J. R.; Lewis, N. S.; Gray, H. B. Will Solar-Driven Water-Splitting Devices See the Light of Day? *Chem. Mater.* **2013**, *26*, 407−414.

DOI: 10.1021/am5067783
ACS Appl. Mater. Interfaces 2015, 7, 1550−1559

(7) Mayer, M. T.; Lin, Y.; Yuan, G.; Wang, D. Forming Heterojunctions at the Nanoscale for Improved Photoelectrochemical Water Splitting by Semiconductor Materials: Case Studies on Hematite. *Acc. Chem. Res.* **2013**, *46*, 1558−1566.
(8) Hardee, K. L.; Bard, A. J. Semiconductor Electrodes: X. Photoelectrochemical Behavior of Several Polycrystalline Metal Oxide Electrodes in Aqueous Solutions. *J. Electrochem. Soc.* **1977**, *124*, 215−224.
(9) Walter, M. G.; Warren, E. L.; McKone, J. R.; Boettcher, S. W.; Mi, Q.; Santori, E. A.; Lewis, N. S. Solar Water Splitting Cells. *Chem. Rev.* **2010**, *110*, 6446−6473.
(10) Chen, Z.; Jaramillo, T. F.; Deutsch, T. G.; Kleiman-Shwarsctein, A.; Forman, A. J.; Gaillard, N.; Garland, R.; Takanabe, K.; Heske, C.; Sunkara, M.; McFarland, E. W.; Domen, K.; Miller, E. L.; Turner, J. A.; Dinh, H. N. Accelerating Materials Development for Photoelectrochemical Hydrogen Production: Standards for Methods, Definitions, and Reporting Protocols. *J. Mater. Res.* **2010**, *25*, 3−16.
(11) Grätzel, M. Photoelectrochemical Cells. *Nature* **2001**, *414*, 338−344.
(12) Hamann, T. W. Splitting Water With Rust: Hematite Photoelectrochemistry. *J. Chem. Soc., Dalton Trans.* **2012**, *41*, 7830−7834.
(13) Klahr, B. M.; Hamann, T. W. Current and Voltage Limiting Processes in Thin Film Hematite Electrodes. *J. Phys. Chem. C* **2011**, *115*, 8393−8399.
(14) Young, K. M. H.; Klahr, B. M.; Zandi, O.; Hamann, T. W. Photocatalytic Water Oxidation with Hematite Electrodes. *Catal. Sci. Technol.* **2013**, *3*, 1660−1671.
(15) Mayer, M. T.; Du, C.; Wang, D. Hematite/Si Nanowire Dual-Absorber System for Photoelectrochemical Water Splitting at Low Applied Potentials. *J. Am. Chem. Soc.* **2012**, *134*, 12406−12409.
(16) Cesar, I.; Sivula, K.; Kay, A.; Zboril, R.; Grätzel, M. Influence of Feature Size, Film Thickness, and Silicon Doping on the Performance of Nanostructured Hematite Photoanodes for Solar Water Splitting. *J. Phys. Chem. C* **2008**, *113*, 772−782.
(17) Barroso, M.; Mesa, C. A.; Pendlebury, S. R.; Cowan, A. J.; Hisatomi, T.; Sivula, K.; Grätzel, M.; Klug, D. R.; Durrant, J. R. Dynamics of Photogenerated Holes in Surface Modified α-Fe_2O_3 Photoanodes for Solar Water Splitting. *Proc. Natl. Acad. Sci. U. S. A.* **2012**, *109*, 15640−15645.
(18) Dare-Edwards, M. P.; Goodenough, J. B.; Hamnett, A.; Trevellick, P. R. Electrochemistry and Photoelectrochemistry of Iron(III) Oxide. *J. Chem. Soc., Faraday Trans. 1* **1983**, *79*, 2027−2041.
(19) Riha, S. C.; Klahr, B. M.; Tyo, E. C.; Seifert, S.; Vajda, S.; Pellin, M. J.; Hamann, T. W.; Martinson, A. B. F. Atomic Layer Deposition of a Submonolayer Catalyst for the Enhanced Photoelectrochemical Performance of Water Oxidation with Hematite. *ACS Nano* **2013**, *7*, 2396−2405.
(20) Klahr, B.; Gimenez, S.; Fabregat-Santiago, F.; Bisquert, J.; Hamann, T. W. Photoelectrochemical and Impedance Spectroscopic Investigation of Water Oxidation with "Co−Pi"-Coated Hematite Electrodes. *J. Am. Chem. Soc.* **2012**, *134*, 16693−16700.
(21) Chatman, S.; Zarzycki, P.; Preočanin, T.; Rosso, K. M. Effect of Surface Site Interactions on Potentiometric Titration of Hematite (α Fe_2O_3) Crystal Faces. *J. Colloid Interface Sci.* **2013**, *391*, 125−134.
(22) Chatman, S.; Zarzycki, P.; Rosso, K. M. Surface Potentials of (001), (012), (113) Hematite (α-Fe_2O_3) Crystal Faces in Aqueous Solution. *Phys. Chem. Chem. Phys.* **2013**, *15*, 13911−13921.
(23) Yanina, S. V.; Rosso, K. M. Linked Reactivity at Mineral-Water Interfaces Through Bulk Crystal Conduction. *Science* **2008**, *320*, 218−222.
(24) Zarzycki, P.; Chatman, S.; Preočanin, T.; Rosso, K. M. Electrostatic Potential of Specific Mineral Faces. *Langmuir* **2011**, *27*, 7986−7990.
(25) Catalano, J. G.; Fenter, P.; Park, C. Interfacial Water Structure on the (012) Surface of Hematite: Ordering and Reactivity in Comparison with Corundum. *Geochim. Cosmochim. Acta* **2007**, *71*, 5313−5324.
(26) Catalano, J. G.; Fenter, P.; Park, C. Water Ordering and Surface Relaxations at the Hematite (110)−Water Interface. *Geochim. Cosmochim. Acta* **2009**, *73*, 2242−2251.
(27) Trainor, T. P.; Chaka, A. M.; Eng, P. J.; Newville, M.; Waychunas, G. A.; Catalano, J. G.; Brown, G. E. Structure and Reactivity of the Hydrated Hematite (0001) Surface. *Surf. Sci.* **2004**, *573*, 204−224.
(28) Hiemstra, T.; Van Riemsdijk, W. H. Effect of Different Crystal Faces on Experimental Interaction Force and Aggregation of Hematite. *Langmuir* **1999**, *15*, 8045−8051.
(29) Hiemstra, T.; Van Riemsdijk, W. H.; Bolt, G. H. Multisite Proton Adsorption Modeling at the Solid/Solution Interface of (Hydr)oxides: A New Approach. *J. Colloid Interface Sci.* **1989**, *133*, 91−104.
(30) Venema, P.; Hiemstra, T.; Weidler, P. G.; van Riemsdijk, W. H. Intrinsic Proton Affinity of Reactive Surface Groups of Metal (Hydr)Oxides: Application to Iron (Hydr)Oxides. *J. Colloid Interface Sci.* **1998**, *198*, 282−295.
(31) Eggleston, C. M.; Hochella, M. F. The Structure of Hematite {001} Surfaces by Scanning Tunneling Microscopy; Image Interpretation, Surface Relaxation, and Step Structure. *Am. Mineral.* **1992**, *77*, 911−922.
(32) Barrón, V.; Torrent, J. Surface Hydroxyl Configuration of Various Crystal Faces of Hematite and Goethite. *J. Colloid Interface Sci.* **1996**, *177*, 407−410.
(33) McCrory, C. C. L.; Jung, S.; Peters, J. C.; Jaramillo, T. F. Benchmarking Heterogeneous Electrocatalysts for the Oxygen Evolution Reaction. *J. Am. Chem. Soc.* **2013**, *135*, 16977−16987.
(34) Zarzycki, P.; Rosso, K. M.; Chatman, S.; Preočanin, T.; Kallay, N.; Piasecki, W. Theory, Experiment and Computer Simulation of the Electrostatic Potential at Crystal/Electrolyte Interfaces. *Croat. Chem. Acta* **2010**, *83*, 457−474.
(35) Boily, J. F.; Chatman, S.; Rosso, K. M. Inner-Helmholtz Potential Development at the Hematite (α-Fe_2O_3) (0 0 1) Surface. *Geochim. Cosmochim. Acta* **2011**, *71*, 4113−4124.
(36) Zarzycki, P.; Preočanin, T. Point of Zero Potential of Single-Crystal Electrode/Inert Electrolyte Interface. *J. Colloid Interface Sci.* **2012**, *370*, 139−143.
(37) Preočanin, T.; Majić, Z.; Kovačević, D.; Kallay, N. Adsorption of Oxalic Acid Onto Hematite: Application of Surface Potential Measurements. *Adsorpt. Sci. Technol.* **2007**, *25*, 429−437.
(38) Preočanin, T.; Čop, A.; Kallay, N. Surface Potential of Hematite in Aqueous Electrolyte Solution: Hysteresis and Equilibration at the Interface. *J. Colloid Interface Sci.* **2006**, *299*, 772−776.
(39) Kallay, N.; Preočanin, T. Measurement of the Surface Potential of Individual Crystal Planes of Hematite. *J. Colloid Interface Sci.* **2008**, *318*, 290−295.
(40) Kallay, N.; Dojnović, Z.; Čop, A. Surface Potential at the Hematite-Water Interface. *J. Colloid Interface Sci.* **2005**, *286*, 610−614.
(41) Pourbaix, M. *Atlas of Electrochemical Eqilibria in Aqueous Solutions;* National Association of Corrosion Engineers: Houston, TX, 1974.
(42) Barbosa, P.; Lagoeiro, L.; Scholz, R.; Graça, L.; Mohallem, N. Magnetite-Hematite Transformation: Correlation Between Natural and Synthetic Features. *Mineral. Petrol.* **2014**, 1−9.
(43) Gajda-Schrantz, K.; Tymen, S.; Boudoire, F.; Toth, R.; Bora, D. K.; Calvet, W.; Gratzel, M.; Constable, E. C.; Braun, A. Formation of an Electron-Hole Doped Film in The α-Fe_2O_3 Photoanode Upon Electrochemical Oxidation. *Phys. Chem. Chem. Phys.* **2013**, *15*, 1443−1451.
(44) Eggleston, C. M.; Stack, A. G.; Rosso, K. M.; Bice, A. M. Adatom Fe(III) on the Hematite Surface: Observation of A Key Reactive Surface Species. *Geochem. Trans.* **2004**, *5*, 33−40.
(45) Shuey, R. T. *Semi-Conducting Ore Minerals;* Elsevier Science: Amsterdam, The Netherlands, 1975.
(46) Rosso, K. M.; Smith, D. M. A.; Dupuis, M. An Ab Initio Model of Electron Transport in Hematite (α-Fe_2O_3) Basal Planes. *J. Chem. Phys.* **2003**, *118*, 6455−6466.

DOI: 10.1021/am5067783
ACS Appl. Mater. Interfaces 2015, 7, 1550−1559

(47) Bertotti, G. *Hysteresis in Magnetism: For Physicists, Materials Scientists, and Engineers;* Academic Press: San Diego, CA, 1998.
(48) Banwart, S.; Davies, S.; Stumm, W. The Role of Oxalate in Accelerating the Reductive Dissolution of Hematite (α-Fe2O3) by Ascorbate. *Colloids Surf.* **1989**, *39*, 303−309.
(49) Xu, Y.; Schoonen, M. A. A. The Absolute Energy Positions of Conduction and Valence Bands of Selected Semiconducting Minerals. *Am. Mineral.* **2000**, *85*, 543−556.
(50) Berube, Y. G.; Onoda, G. Y.; de Bruyn, P. L. Proton Adsorption at the Ferric Oxide/Aqueous Solution Interface II. Analysis of Kinetic Data. *Surf. Sci.* **1967**, *8*, 448−461.
(51) Onoda, G. Y.; de Bruyn, P. L. Proton Adsorption at the Ferric Oxide/Aqueous Solution Interface I. A Kinetic Study od Adsorption. *Surf. Sci.* **1966**, *4*, 48−63.
(52) Zarzycki, P.; Rosso, K. M. Nonlinear Response of the Surface Electrostatic Potential Formed at Metal Oxide/Electrolyte Interfaces. A Monte Carlo Simulation Study. *J. Colloid Interface Sci.* **2010**, *341*, 143−152.
(53) Espenson, J. H. *Chemical Kinetrics and Reaction Mechanisms,* 2nd ed.; McGraw-Hill: New York, 1995.
(54) Connors, K. A. *Chemical Kinetics: The Study of Reaction Rates in Solution;*Wiley-VCH: Weinheim, Germany, 1993; p 479.
(55) Neamen, D. *An Introduction to Semiconductor Devices;* McGraw-Hill: New York, 2006.
(56) Sze, S. M.; Ng, K. K. *Physics of Semiconductor Devices,* 3rd ed.; Wiley: Hoboken, New Jersey, 2007.
(57) Butler, M. A.; Ginley, D. S. Prediction of Flatband Potentials at Semiconductor-Electrolyte Interfaces from Atomic Electronegativities. *J. Electrochem. Soc.* **1978**, *125*, 228−232.
(58) Schrebler, R.; Bello, K.; Vera, F.; Cury, P.; Muñoz, E.; del Río, R.; Gómez Meier, H.; Córdova, R.; Dalchiele, E. A. An Electrochemical Deposition Route for Obtaining α-Fe_2O_3 Thin Films. *Electrochem. Solid-State Lett.* **2006**, *9*, C110−C113.
(59) Glasscock, J. A.; Barnes, P. R. F.; Plumb, I. C.; Savvides, N. Enhancement of Photoelectrochemical Hydrogen Production from Hematite Thin Films by the Introduction of Ti and Si. *J. Phys. Chem. C* **2007**, *111*, 16477−16488.
(60) Leland, J. K.; Bard, A. J. Photochemistry of Colloidal Semiconducting Iron Oxide Polymorphs. *J. Phys. Chem.* **1987**, *91*, 5076−5083.
(61) Mulvaney, P.; Swayambunathan, V.; Grieser, F.; Meisel, D. Dynamics of Interfacial Charge-Transfer in Irin(III) Oxide Colloids. *J. Phys. Chem.* **1988**, *92*, 6732−6740.
(62) Mulvaney, P.; Cooper, R.; Grieser, F.; Meisel, D. Charge Trapping in the Reductive Dissolution of Colloidal Suspensions of Iron(III) Oxides. *Langmuir* **1988**, *4*, 1206−1211.
(63) Grundmann, M. *The Physics of Seminconductors: An Introduction Including Nanoparticles and Applications;* Springer-Verlag: Berlin, 2010; p 864.
(64) Burstein, E. Anomalous Optical Absorption Limit in InSb. *Phys. Rev.* **1954**, *93*, 632−633.
(65) Brillet, J.; Yum, J.-H.; Cornuz, M.; Hisatomi, T.; Solarska, R.; Augustynski, J.; Graetzel, M.; Sivula, K. Highly Efficient Water Splitting by a Dual-Absorber Tandem Cell. *Nat. Photonics* **2012**, *6*, 824−828.
(66) Le Formal, F.; Tétreault, N.; Cornuz, M.; Moehl, T.; Grätzel, M.; Sivula, K. Passivating Surface States on Water Splitting Hematite Photoanodes With Alumina Overlayers. *Chem. Sci.* **2011**, *2*, 737−743.

DOI: 10.1021/am5067783
ACS Appl. Mater. Interfaces 2015, 7, 1550−1559